Emergence and control of breather and plasma oscillations by synchronizing perturbations

L. Friedland
Racah Institute of Physics, Hebrew University of Jerusalem, Jerusalem 91904, Israel

A. G. Shagalov
Institute of Metal Physics, Ekaterinburg 620219, Russian Federation

(Received 1 March 2006; published 12 June 2006)

Large amplitude standing waves of spatially periodic sine-Gordon equations are excited and controlled by sweeping the frequency of a small, spatially modulated driving oscillation through resonances in the system. The approach is based on capturing the system into resonances and subsequent adiabatic, persistent phase locking (autoresonance) yielding control via a single external parameter (the driving frequency). Plasma oscillations in the system are excited by using a small amplitude drive in the form of a chirped frequency standing wave, while emergence of autoresonant breather oscillations requires driving by a combination of small amplitude oscillation and standing waves.

DOI: 10.1103/PhysRevE.73.066612 PACS number(s): 05.45.Yv, 05.45.Xt, 89.75.Kd, 52.35.Mw

I. INTRODUCTION

Nonlinear wave equations in fluids and plasmas frequently have different classes of solutions. Suppose, one desires to generate (experimentally or in simulations) a wave form u of a particular class in a system governed by wave equation $\hat{N}(u)=0$ ($\hat{N}$ being a nonlinear spatiotemporal differential operator). The standard procedure for achieving this goal requires accurate realization of some nontrivial initial/boundary conditions. Alternatively, in searching for a more realizable approach, one can start from trivial initial/boundary conditions, but consider a perturbed problem $\hat{N}(u)=\varepsilon f$, where $\varepsilon \ll 1$ and f is a function on space time. Can one find a *simple* f, such that u in the perturbed system arrives at a vicinity of the desired nontrivial solution in the process of evolution? Recently, this question was addressed in the context of excitation of multiphase waves of the Korteweg-de Vries (KdV) and nonlinear Schrodinger (NLS) equations [1,2]. Here, we pose a similar problem in application to the periodic sine-Gordon (SG) system, i.e., study the driven SG problem

$$u_{tt} - u_{xx} + \sin u = \varepsilon f(x,t), \tag{1}$$

where both field u and the driving function f are subject to periodic boundary conditions $u(x,t)=u(x+L,t)$, $f(x,t)=f(x+L,t)$. The sine-Gordon equation ($\varepsilon=0$) is one of the most important equations of nonlinear physics and describes many physical applications [3]. It has a variety of solutions, a *single* phase wave train, $u(x,t)=u(\theta)$, $\theta=kx-\omega t$, being the simplest example. If one adds periodic boundary condition, standing SG wave solutions exist of form [4]

$$u(x,t) = 4\tan^{-1}[F(x)G(t)], \tag{2}$$

where $F(x)$ and $G(t)$ are expressed in terms of Jacobian elliptic functions, which are periodic in x and t, respectively. Well known realizations of Eq. (2) are *breather* and *plasma oscillations*. In the breather case $F(x)=A\mathrm{dn}[\beta x,m_1]$ and $G(t)=\mathrm{sn}(\gamma t,m_2)$, while, for plasma oscillations, $F(x)=A\mathrm{cn}[\beta x,m_1]$ and $G(t)=\mathrm{cn}(\gamma t,m_2)$. There are five constants in the definition of each of these standing waves, i.e., β,γ, "amplitude" A, and moduli $m_{1,2}$ of the elliptic functions, but only *two* of these constants (say $m_{1,2}$) are independent, while others are related algebraically. For example, in the breather case [5], $\beta=\gamma A$ (the dispersion relation) and $A^2(1-m_1^2)=m_2^2/A^2=(\gamma^2+\beta^2)^{-1}-1$. For plasma oscillations, in contrast [5], the dispersion relation is $\gamma^2-\beta^2=(1-A^2)/(1+A^2)$, while $\beta^2(m_1^2-A^2)=\gamma^2(A^2-m_2^2)=A^2(1+A^2)^{-2}$. Note that Eq. (2) represents the simplest *two-phase* solutions of the SG equation. Their two-phase structure can be emphasized by using the notation $u=U(\theta_1,\theta_2;m_1,m_2)$, where U is 2π periodic with respect to phase variables $\theta_1(x)$ and $\theta_2(t)$, describing oscillations of either $F(x)$ or $G(t)$. The wave numbers associated with the spatial oscillations are $\kappa\equiv\theta_{1x}=\pi\beta/K(m_1)$ and $\pi\beta/[2K(m_1)]$ in the breather and plasma cases, respectively, K is the complete elliptic integral of the first kind, while the frequency of temporal oscillations in both cases is $\Omega\equiv\theta_{2t}=\pi\gamma/[2K(m_2)]$. In this work we seek simple perturbations εf in (1), yielding excitation of large amplitude breather or plasma oscillations, starting from *zero* initial conditions. Small amplitude limits of these waves are important in this context. Plasma oscillations reduce to linear standing waves $u=A\cos(\kappa x)\cos(\Omega t)$ as $A\to 0$. In contrast, breathers exist for $\kappa<1$ only, and their amplitudes are *finite,* $A>A_{\min}=\kappa^{-1}-(\kappa^{-2}-1)^{1/2}$. Nevertheless, for smaller A, a spatially uniform solution $u(t)=4\tan^{-1}[A\mathrm{sn}(\gamma t,m_2)]$ (pendulum oscillations), having linear limit $u(t)=A\sin(\Omega t)$, can be viewed as a reduced ($m_1=0$) form of breather oscillations.

Now we outline our idea of controlling breather and plasma oscillations by adiabatic synchronization. Let the perturbing function in Eq. (1) be an oscillation $f=f_0(x)\cos\int\omega(t)dt$ having slowly varying (chirped) frequency $\omega(t)$ and spatially modulated amplitude $f_0(x)=f_0(x+L)$. Then, assume that the driven system allows an approximate *synchronized* solution of form (2), where parameters are slow functions of time, such that this solution is phase locked with the drive at *all* times. In other words, we assume $u\approx U(\theta_1,\theta_2;m_1,m_2)$, where $m_{1,2}$ and $\Omega=\theta_{2t}$ are slow functions of time (the wave number $\kappa=\theta_{1x}$ is constant due to periodic boundary conditions) such that $\theta_1\approx 2\pi x/L$ (assum-

ing lowest order spatial mode) and $\theta_2 \approx \int \omega(t)dt$ at all times. The phase locking assumption means matching of the wave numbers and frequencies, i.e., $\kappa = 2\pi/L$ and $\Omega \approx \omega(t)$. This, in turn, yields two additional algebraic constrains on parameters $m_{1,2}$ of the standing wave, while its phases $\theta_{1,2}$ are also known approximately by phase locking assumption. Therefore, if the above-mentioned synchronized solution exists, it is fully controlled by a single external parameter [the frequency $\omega(t)$ of the driving perturbation], allowing excursion in the solutions space of the nonlinear system. We shall see below that under certain conditions, the passage through resonances in the driven SG system yields the desired persistent phase locking between slowly varying driving perturbations (synchronizing perturbations in the following) and subsequent emergence of large amplitude standing waves. The analysis of this excitation process comprises the main goals of the present work.

The periodic, ac-driven SG system was studied in the past for *constant* frequency drives [6]. The idea of passage through resonance and subsequent synchronization for exciting *single* phase SG wave trains was suggested more recently [7]. The theory in this case used Whitham's single-phase averaged variational principle [8] describing adiabatic evolution of the excited synchronized state. A similar approach was also applied to studying nonlinear mode conversion in the system of two weakly coupled SG equations with slow parameters [9]. The present work comprises an extension of the idea of control of SG waves by synchronizing, *varying frequency* perturbations to the simplest multiphase solutions, i.e., breather and plasma oscillations. Recently, Khomeriki and Leon [10] suggested a different synchronization approach to excitation of these solutions. They studied constant frequency, but *varying amplitude* oscillating boundary condition in the SG problem and used different forms of variation of the amplitude and weak *damping* to arrive at one of the two stable attractors in the system. Here, we consider undamped, perturbatively driven SG system and suggest recipes for excitation of these solutions by passage through resonances. Our presentation will be as follows. Section II will demonstrate excitation and control of large amplitude standing SG waves by chirped frequency perturbations in numerical simulations, focusing on plasma and breather oscillation cases separately. Section III will consider synchronized evolution in more detail. In particular, we shall study conditions for phase locking in our adiabatically driven systems and use a weakly nonlinear variant of Whitham's averaged variational principle in analyzing characteristic thresholds on the driving amplitudes for capturing standing SG waves into resonances. Finally, in Sec. IV we will present our conclusions.

II. ADIABATIC SYNCHRONIZATION VIA NUMERICAL SIMULATIONS

A. Synchronized plasma oscillations

We proceed by illustrating the idea of controlling plasma oscillations by synchronization in simulations. We solved Eq. (1) numerically, subject to zero initial and periodic boundary conditions. The simulation used a standard pseudospectral method [11]. The accuracy of the solution was tested by varying the number of spatial harmonics and the time step. Our driving perturbation was a small amplitude standing wave

$$\varepsilon f(t) = \varepsilon \cos(2\pi x/L)\cos \int \omega(t)dt. \tag{3}$$

The driving frequency in Eq. (3) decreased linearly in time, $\omega(t) = \omega_0 - \alpha t$ ($\alpha \ll 1$), passing, at $t=0$, the linear resonance, $\omega = \omega_0 = [(2\pi/L)^2 + 1]^{1/2}$, with small amplitude plasma oscillations of the ideal ($\varepsilon = 0$) SG system.

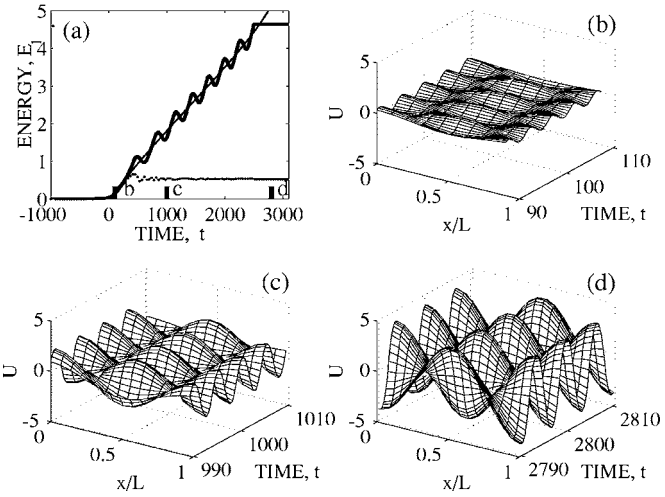

FIG. 1. The emergence of plasma oscillations by synchronization. (a): Energy E_1 versus time (thick line). The ideal synchronized state is shown by a thin line. The dotted line represents evolution of E_1 in simulations for ϵ slightly below threshold. (b), (c), and (d): The numerical wave forms in three small time windows of duration $\Delta t = 20$ at different stages of evolution. Location of these windows is shown by bars on the t axis in (a).

The simulation results presented in Figs. 1(a)–1(d) illustrate a large amplitude standing wave emerging from zero after passage through resonance. The thick line in Fig. 1(a) shows the evolution of "energy" $E_1 = \langle 0.5(u_t^2 + u_t^2) - \cos u \rangle_L + 1$, where $\langle \cdots \rangle_L = L^{-1} \int_0^L (\cdots) dx$ represents averaging over one spatial period. The energy is time independent for plasma oscillations of the ideal SG system (see the Appendix) and its increase with the decrease of the driving frequency $\omega(t)$ indicates excitation of a growing amplitude wave. We used the parameters $L=7$, $\alpha = 1.5 \times 10^{-4}$, $\varepsilon = 8.25 \times 10^{-3}$, and initial time $t_{in} = -1000$ in our simulations and switched off the driving function at $t = t_f = 2500$ (note that E_1 remains constant beyond this time). Figures 1(b)–1(d) show the actual numerical wave forms as observed in three narrow time windows of duration $\Delta t = 20$ at different stages of excitation. The short bars on the t axis in Fig. 1(a) indicate positions of these windows, i.e., just beyond the linear resonance [$t=100$, Fig. 1(b)], at some intermediate stage [$t=1000$, Fig. 1(c)], and at $t = 2800 > t_f$ [Fig. 1(d)]. These results show that the excited wave is indeed continuously phase locked in both space and time with the driving standing wave. The spatial phase locking (the location of the wave maxima remains at $x = L/2$ at all

times) is obvious, while one also notices that the frequency of temporal oscillations of the wave form decreases as one passes from Fig. 1(b), through Fig. 1(c) to Fig. 1(d), following the decrease of the driving frequency. One also finds numerically that the growing amplitude wave [as in Figs. 1(b)–1(d)] beyond the linear resonance emerges only if the driving amplitude exceeds a threshold. Theoretically, this threshold scales as $\varepsilon_{th}=3.8\omega_0^{1/2}\alpha^{3/4}$ [see Eq. (27) in Sec. III]. In our case, $\varepsilon_{th}=8\times10^{-3}$, so $\varepsilon=8.25\times10^{-3}$ in simulations [the thick solid line in Fig. 1(a)] is slightly above the threshold. The dotted line in Fig. 1(a) shows a similar simulation, but for $\varepsilon=7.95\times10^{-3}$, i.e., just below the threshold. We see that the energy in this case saturates at some relatively low value. The simulations also showed that the phase locking between the wave and the drive in this case was destroyed near the linear resonance. Furthermore, we found that if the driving field is switched off as in Fig. 1, the resulting solution remains numerically stable for times much longer than those shown in the figure. Nevertheless, if the drive is present beyond t_f, but the driving frequency remains constant, the excited wave remains phase locked with the drive for some time, but then develops an instability, destroying the phase locking at later times. This instability growth rate increases with ε, so reaching larger plasma oscillation energies by synchronization approach requires smaller ε and, therefore, smaller driving frequency chirp rate due to the threshold phenomenon. In order to qualitatively test the form of the excited wave and synchronization in the system, we have assumed the existence of an ideal synchronized state beyond the linear resonance, as described in the Introduction, and found parameters of this state by solving the system of algebraic equations

$$\gamma^2-\beta^2=(1-A^2)/(1+A^2), \tag{4}$$

$$\beta^2(m_1^2-A^2)=\gamma^2(A^2-m_2^2)=A^2(1+A^2)^{-2}, \tag{5}$$

$$\beta=4K(m_1)/L; \quad \gamma=4K(m_2)\omega(t). \tag{6}$$

Then, we substituted these parameters in the expression for the energy of plasma oscillations of the perfect SG equation (see the Appendix)

$$E_1=8A^2\gamma^2m_1^{-2}(1-m_2^2)[m_1^2-1+E(m_1)/K(m_1)], \tag{7}$$

where E is the complete elliptic integral of the second kind, and presented the results in Fig. 1(a) by a thin line. We observe that beyond linear resonance, E_1 in simulations (the thick line) performs small oscillations around a monotonically growing energy predicted via the ideal persistent synchronization assumption. We shall show below that these oscillations comprise the characteristic signature of phase locking in the driven system and that the frequency of the oscillations scales as $\varepsilon^{1/2}$. This completes our numerical illustration of synchronized plasma oscillations and we proceed to the excitation of periodic SG breathers.

B. Synchronized breather oscillations

In forming periodic SG breathers by synchronization we again start from zero initial conditions. However, breathers do not have a linear limit, and, therefore, one needs a different driving strategy. The idea is to excite spatially a uniform solution, $u(t)=4\tan^{-1}[A\mathrm{sn}(\gamma t,m_2)]$ (pendulum oscillations), of the SG equation first (these oscillations have a linear limit) and adiabatically transform this solution into a breather at a later stage. This goal is achieved by using a spatially modulated driving oscillation of the form

$$\varepsilon f(x,t)=\varepsilon[1+r\cos(k_0x)]\cos\int\omega(t)dt, \tag{8}$$

where the driving frequency $\omega(t)$ decreases, passing the linear resonance with pendulum oscillations ($\omega=1$), and we shall again use a linear frequency sweep, $\omega(t)=1-\alpha t$, in the simulations. Parameter r characterizing the spatial modulation in the drive is kept to zero for $t<0$, but is switched to $r=1$ at $t=0$ and stays constant at later times. The reason for having $r=0$ prior to the linear resonance is to prevent passage through $\omega=\omega_0=[(2\pi/L)^2+1]^{1/2}$ resonance yielding excitation of the plasma oscillations, as described above. Thus, we employ a different resonance, yielding excitation of a different solution branch. We again solve Eq. (1) numerically, using zero initial (at $t_{in}=-1000$) and periodic boundary conditions and present the simulation results in Fig. 2.

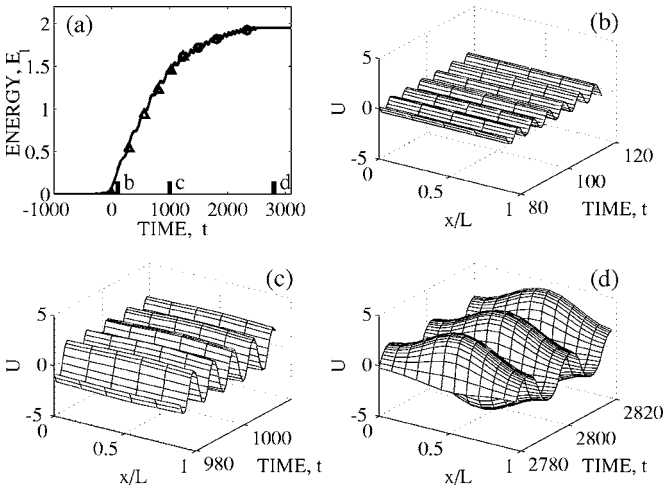

FIG. 2. The emergence of breather oscillations by a synchronizing perturbation. (a): Energy E_1 versus time (solid line). The ideal synchronized state is shown by triangles ($A<A_{min}$) and circles ($A>A_{min}$). (b), (c) and (d): The wave forms in three time windows of duration $\Delta t=40$ at different stages of evolution. Location of these windows is shown by bars on the t axis in (a). One observes excitation of a uniform time-synchronized state in (b) and (c), while (d) corresponds to a spatiotemporally synchronized breather state.

Figure 2(a) shows the evolution of energy E_1. We use parameters $L=7$, $\alpha=2.5\times10^{-4}$, $\varepsilon=12\times10^{-3}$ and switch off the driving function at $t=t_f=2500$ (E_1 again remains constant beyond this time). Figures 1(b)–1(d) show the actual numerical wave forms as observed in three narrow time windows of duration $\Delta t=40$ at different stages of excitation. The bars on the t axis in Fig. 3(a) indicate the positions of these windows, i.e., just beyond the linear resonance [$t=100$, Fig. 2(b)], at $t=1000$ [Fig. 2(c)], and $t=2800>t_f$ [Fig. 2(d)]. We observe the emergence of a nearly uniform solution after the passage

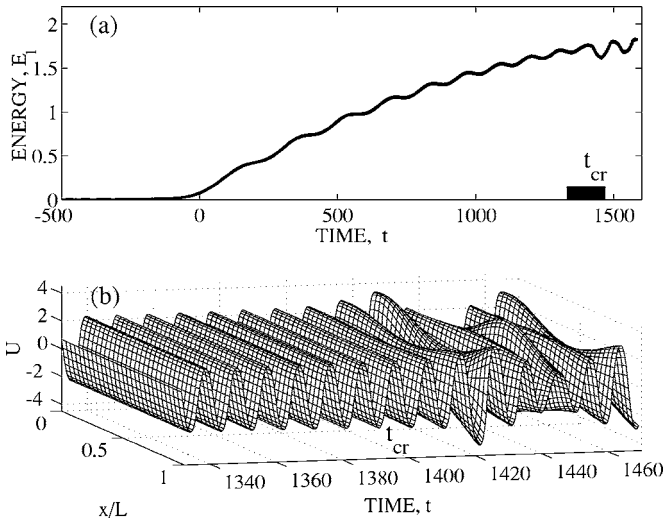

FIG. 3. The modulational instability of a synchronized uniform state. (a): The evolution of energy E_1 for vanishing spatial modulation parameter r in the driving function. The excited temporally synchronized state becomes unstable at $t=t_{cr}$ as the amplitude A of the driven solution exceeds A_{min} for existence of breather oscillations. (b): The wave form at the onset of modulational instability in a time window [indicated by a bar on the t axis in (a)] around t_{cr}.

through resonance in Figs. 2(b) and 2(c). The spatial modulation in the drive is *nonresonant* at this stage and has little effect on the excitation process. Consequently, we form a growing amplitude solution of $u_{tt}+\sin u=\varepsilon\cos\int\omega(t)dt$ by passage through resonance. This adiabatically driven pendulum problem was studied earlier [7]. It was shown that the synchronization (phase locking) followed by efficient excitation of the pendulum to high energies and approach to separatrix, is possible, as the amplitude of oscillations approaches π for $\omega(t)\to 0$, provided the driving amplitude ε is large enough. We shall make this statement more accurate in Sec. III showing that similarly to the plasma oscillations case, ε must exceed a sharp threshold, $\varepsilon_{th}=3.3\alpha^{3/4}$ [see Eq. (32) in Sec. III], for excitation of a synchronized spatially uniform SG solution. In terms of our breather solution, the uniform solution corresponds to a situation, where $m_1=0$. Consequently, beyond the linear resonance ($t>0$), all parameters are functions of time only, $u=u(t)\approx 4\arctan[A\mathrm{sn}(\gamma t,m_2)]$, where $m_2\approx A^2$, $\gamma(1+A^2)\approx 1$ and, in the synchronized state, $\Omega\approx 4\,\mathrm{K}(m_2)/\gamma\approx\omega(t)$. These three algebraic relations define the ideal, temporally synchronized solution emerging beyond the linear resonance in Figs. 2(b) and 2(c).

The character of the solution in Fig. 2 changes when amplitude A of the excited wave exceeds (at $t=t_{cr}\approx 1400$) a critical value depending on the periodicity length L of the system. We see that the solution in Fig. 2(d) develops a significant spatial modulation. We also find in simulations that the transition from uniform to spatially modulated case occurs for $L>2\pi$ only ($L=7$ in our example) and that the critical value of A coincides with the minimum amplitude $A_{\min}=\kappa^{-1}-(\kappa^{-2}-1)^{1/2}$, $\kappa=2\pi/L$ for the existence of breather oscillations. Furthermore, the emerging beyond the $A_{\min}$ spatially modulated state is, in fact, the desired breather oscillation synchronized with the drive (see below). The excitation of the synchronized breather state [as illustrated in Fig. 2(d)] required a nonvanishing modulation parameter r at t_{cr} in the driving function. Indeed, Fig. 3 shows simulation results for the same parameters and initial conditions as in Fig. 2, but $r=0$ at all times.

One observes the saturation of energy [Fig. 3(a)] as the driven uniform state becomes modulationally unstable beyond t_{cr}. The actual wave form at the onset of the instability (in the time widow $\Delta t=120$ around t_{cr}) is shown in Fig. 3(b). The modulational instability of the uniform state of the ideal SG equation is well known [12]. The temporal synchronization in our simulations allows a slow approach to modulationally unstable region. At the onset of instability of the uniform solution, the amplitude A is the same as the minimum amplitude $A_{\min}$ of the breather solution, while the spatial period of small oscillations of $F(x)$ in the breather (2) is equal to periodicity length L in the problem, i.e., $\kappa=\pi\beta/K(m_1^2\approx 0)\approx 2\gamma A_{\min}=2\pi/L$ [12]. Therefore, the modulational instability of a temporally synchronized state in the driven system proceeds at time $t=t_{cr}$ such that a new spatiotemporal resonance condition is satisfied in the system, i.e., $\kappa=2\pi/L$ and $\Omega=\omega(t)$. The addition of spatial modulations in the drive affects the nonlinear development of the resonantly driven wave, prevents development of modulational instability, and leads to the emergence of a stable, growing amplitude breather oscillation, as the spatiotemporal synchronization continues despite a variation of the driving frequency. The temporal synchronization is seen in the sequence of the wave forms in Figs. 2(b)–2(d), where the decrease of the frequency of the driven wave reflects the decrease of the driving frequency. The spatial synchronization beyond t_{cr} is reflected in the spatial symmetry of the emerging breather oscillations with respect to the center ($x/L=0.5$) of the periodicity length, the same symmetry characterizing spatial modulations of the driving function. A quantitative test of the synchronization can be performed by comparing our simulation results for E_1 [solid line in Fig. 2(a)] with those for breather oscillations of the ideal SG equation [Δ and *circles* in Fig. 2(a)] given by (see the Appendix)

$$E_1=8\gamma^2A^2E(m_1)/K(m_1), \tag{9}$$

where one uses parameters of the ideal spatiotemporally synchronized solution. The parameters in this formula are given by a set of algebraic equations (see the Introduction):

$$\beta=\gamma A;\quad \beta=2K(m_1)/L;\quad \pi\gamma=2K(m_2)\omega(t); \tag{10}$$

$$A^2(1-m_1^2)=m_2^2/A^2=(\gamma^2+\beta^2)^{-1}-1. \tag{11}$$

This system yields a solution for $A>A_{\min}$ only and the corresponding E_1 is shown by *circles* in Fig. 2(a). For $A<A_{\min}$ we set $m_1=0$ (this is the temporally synchronized uniform state), so the second equation in (10), describing spatial synchronization, is irrelevant, leaving us with a simplified system

$$\pi\gamma=2K(m_2)\omega(t);\quad m_2=A^2;A^2+1=\gamma^{-1} \tag{12}$$

for m_2, A, and γ. The solution of this system, substituted into

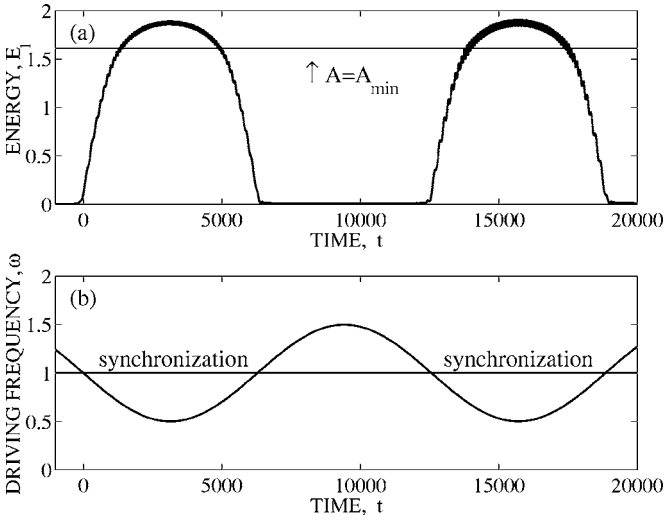

FIG. 4. Two successive excitation and deexcitation stages of synchronized breather oscillations controlled by an oscillating driving frequency. (a) The energy E_1 versus time. The horizontal line shows E_1 corresponding to $A=A_{min}$. Breather oscillations exist in regions $A>A_{min}$ only. (b): The driving frequency ω versus time. Synchronization intervals correspond to $\omega<1$. The drive is out of resonance for $\omega>1$, so E_1 is small in the corresponding time intervals.

(9) yields E_1 shown by the *triangles* in Fig. 2(a). At $A=A_{\min}$, the solution of (12) passes continuously to that of Eqs. (10) and (11) and the wave transforms into a breather oscillation. Figure 2(a) shows a good agreement between the time averaged evolution of E_1 from the simulations and that predicted by the ideal persistent synchronization assumption.

Our final calculation will illustrate that the choice of *linear* frequency chirp is not essential for emergence of synchronized states of the driven SG system. We find that any monotonically decreasing driving frequency, passing through the linear resonance, yields synchronization, provided its rate of variation is small enough. Furthermore, if excited, the synchronized solution $u(x,t)$ can be returned to its nearly vanishing initial state by simply reversing the direction of slow variation of the driving frequency. We illustrate these effects in Fig. 4(a), showing energy E_1 of the solution excited by the driving perturbation of form (8) having an *oscillating* frequency [Fig. 4(b)], $\omega(t)=1-a\sin(\alpha t/a)$, $0<a<1$. For $\alpha t \ll 1$, as before, $\omega(t)\approx 1-\alpha t$, but the driving frequency reaches its minimum at $t=t_1=\pi a/(2\alpha)$ and returns to a linearly resonant value, $\omega=1$, at $t=2t_1$. Figure 4(a) shows the evolution of energy for two successive periods of oscillations of the driving frequency. The parameters in these simulation were $L=7$, $\alpha=2.5\times10^{-4}$, $\varepsilon=1.5\times10^{-2}$, $a=0.5$, and we used zero initial conditions (at $t_0=-t_1/2$). In order to prevent the excitation of plasma oscillations, we again set the modulation parameter $r=0$ in (8) in time intervals, where $\omega(t)>1$, while $r=1$ for $\omega(t)<1$. We see two periods of excitation and deexcitation of the synchronized state in the figure. The energy of the solution is small when $\omega(t)>1$, since the driving perturbation is out of resonance in these regions. In contrast, when $\omega(t)<1$, we excite a temporally synchronized uniform state until $A<A_{\min}$ [the energy level corresponding to $A_{\min}$ is shown by the horizontal line in Fig. 4(a)]. This state transforms into a spatiotemporally synchronized breather state for $A>A_{\min}$ and the whole process is repeated twice as the driving frequency goes in and out of resonance in successive oscillations. This illustration shows that by establishing synchronization in the system, one is able to control the emerging standing wave via a single external parameter, i.e., the frequency of the driving perturbation. Next, we present our theory of the aforementioned thresholds for adiabatic synchronization of standing SG waves.

III. SYNCHRONIZATION THRESHOLDS

A. Plasma oscillations

The threshold for synchronization by passage through resonance is a weakly nonlinear phenomenon and can be conveniently studied by using a weakly nonlinear version of the Whitham's averaged variational principle [8], adopted to our autoresonantly driven system. To this end, the driven problem (1) is formulated via the variational principle

$$\delta \int L dx dt = 0, \tag{13}$$

where, in the weakly nonlinear limit,

$$L(u,u_x,u_t;x,t) = \frac{1}{2}(u_t^2 - u_x^2 - u^2) + \frac{1}{24}u^4 + \varepsilon u f(x,t), \tag{14}$$

and $f(x,t)=\cos(k_0 x)\cos\int\omega(t)dt$. We assume a slow variation of the driving frequency $\omega(t)$, and, seeking an adiabatically phase-locked plasma oscillation in the problem, and adopt the following two-scale representation:

$$u = u_0(t) + u_1(t)\cos(\theta_1)\cos(\theta_2) + u_2(t)\cos^2(\theta_1)\cos^2(\theta_2), \tag{15}$$

where the time dependence in the amplitudes $u_i(t)$ is slow, the phases $\theta_1(x)=k_0 x$, $\theta_2=\theta_2(t)$ are fast, but the associated wave number $k_0=2\pi/L$ is constant, and the frequency $\Omega(t)=d\theta_2/dt$ is a slow function of time. Furthermore, since the standing wave solution for the linear unperturbed problem is $u=u_1\cos(\theta_1)\cos(\theta_2)$, $u_1=$const, we order $u_{0,2}$ in Eq. (15) as $O(u_1^2)$. We have already assumed phase locking between θ_1 and the spatial driving phase $k_0 x$. We shall also assume that the second phase, θ_2, is locked with the driving phase $\int\omega(t)dt$, but allow a *small* and *slow* mismatch $\Phi(t)=\theta_2-\int\omega(t)dt$ in the problem. The goal is to set up a procedure for finding *slow* amplitudes $u_i(t)$ and phase mismatch $\Phi(t)$.

Following Whitham's approach [8], we substitute our two-scale representation (15) into Eq. (14) and average the result with respect to the fast phase variables, viewing the slow time in the problem fixed. This yields an averaged Lagrangian

$$\langle L\rangle_{\theta_{1,2}} = \Lambda(u_0,u_1,u_2;\theta_2,\theta_{2t}) = \Lambda_a + \Lambda_b + \frac{\varepsilon}{2}u_1\cos\Phi, \tag{16}$$

where

$$\Lambda_a = \frac{1}{8}(\Omega^2 - k_0^2 - 1)u_1^2$$

and

$$\Lambda_b = \frac{3}{512}u_1^4 + \frac{3}{32}u_2^2\left(\Omega^2 - k_0^2 - \frac{9}{4}\right) - \frac{1}{2}u_0\left(u_0 + \frac{1}{2}u_2\right).$$

Note that θ_2 enters directly in Eq. (16) through Φ in the driving term, but also via $\Omega = d\theta_2/dt$. By Whitham's approach, the averaged Lagrangian (16) serves in the averaged variational principle

$$\delta \int \Lambda dx dt = 0 \tag{17}$$

yielding the desired equations. For example, variations with respect to u_0 and u_2 in (17) yield

$$u_0 + \frac{1}{4}u_2 = 0, \tag{18}$$

$$\frac{3}{16}u_2^2\left(\Omega^2 - k_0^2 - \frac{3}{4}\right) - \frac{1}{4}u_0 = 0. \tag{19}$$

The lowest order of (19) gives $u_0=0$, and, therefore, from (18), $u_2=0$. Similarly, the variation with respect to u_1 yields

$$\frac{1}{4}(\Omega^2 - \omega_0^2)u_1 + \frac{3}{128}u_1^3 + \frac{\varepsilon}{2}\cos\Phi = 0, \tag{20}$$

where $\omega_0=(k_0^2+1)^{1/2}$ is the linear response frequency of the unperturbed system. Assuming a small departure from resonance, $\Omega \approx \omega_0$, we rewrite Eq. (20) as follows:

$$\Omega = \frac{d\theta_2}{dt} \approx \omega_0 - \frac{3}{64\omega_0}u_1^2 - \frac{\varepsilon}{2\omega_0 u_1}\cos\Phi, \tag{21}$$

or for the phase mismatch,

$$\frac{d\Phi}{dt} = \frac{d\theta_2}{dt} - \omega = \alpha t - \frac{3}{64\omega_0}u_1^2 - \frac{\varepsilon}{2\omega_0 u_1}\cos\Phi, \tag{22}$$

where $\omega=\omega_0-\alpha t$ is used for the driving frequency. Finally, we take variation in (17) with respect to θ_2, yielding, to lowest order, the desired evolution equation for u_1:

$$\frac{du_1}{dt} = -\frac{\varepsilon}{2\omega_0}\sin\Phi. \tag{23}$$

Equations (22) and (23) comprise a closed set of two slow equations for the phase mismatch and amplitude of the driven standing wave. We notice the possibility of having a phase-locked, growing amplitude solution of this system beyond linear resonance ($t>0$). Indeed, by requesting

$$\frac{d\Phi}{dt} \approx \alpha t - \frac{3}{64\omega_0}u_1^2 \approx 0, \tag{24}$$

one has $u_1 \approx \bar{u}_1 \equiv (8\sqrt{\alpha\omega_0/3})t^{1/2}$. In studying the stability of this solution, we write $u_1 \approx \bar{u}_1 + \delta u_1$, ($\bar{u}_1$ is viewed as slow and $|\delta u_1| \ll \bar{u}_1$), differentiate Eq. (24) and substitute Eq. (23) to get

$$\frac{d^2\Phi}{dt^2} \approx \alpha + \frac{3\varepsilon\bar{u}_1}{128\omega_0^2}\sin\Phi. \tag{25}$$

For $\alpha \ll \nu^2 = \frac{3\varepsilon\bar{u}_1}{128\omega_0^2}$ this equation predicts solutions oscillating at frequency $\nu \sim O(\varepsilon^{1/2})$ around a small averaged value, i.e., phase locking in the system. These oscillations of Φ lead to the characteristic oscillating modulations of the energy, seen in Fig. 1(a), as the energy increases in the phase-locked regime of excitation. But, how does one get into this adiabatically synchronized state by passage through the linear resonance? This question leads to the problem of thresholds which is discussed next.

Define new time and amplitude variables, $\tau=\alpha^{1/2}t$ and $A = \frac{1}{8}\alpha^{-1/4}\left(\frac{3}{\omega_0}\right)^{1/2}u_1$ and introduce complex function $\Psi = A\exp(i\Phi)$. A simple test shows that Ψ is described by a nonlinear Shroedinger-type equation

$$i\frac{d\Psi}{d\tau} + (\tau - |\Psi|^2)\Psi = \mu, \tag{26}$$

where $\mu = \frac{\sqrt{3}}{16}\varepsilon\omega_0^{-3/2}\alpha^{-3/4}$. We seek the asymptotic solutions of this equation at large positive τ subject to zero initial Ψ at $\tau=-\infty$. This would describe the passage through resonance (at $t=0$) in our system. There exist two such asymptotic solutions, the bounded solution $\Psi=\Psi_0\exp(i\tau^2/2)$, where Ψ_0 =const and phase mismatch $\Phi=\tau^2/2$ increases in time, and the unbounded solution $\Psi=\tau^{1/2}$, where $\Phi=0$. It is this phase-locked, growing amplitude solution, which describes the capture into resonance and synchronization in our system. But, how the system chooses between the saturated (bounded) and the growing synchronized solutions by starting from zero at $t-\infty$? The answer is simple: the bifurcation is controlled by the *single* parameter μ in the problem. Indeed, the analysis of Eq. (26) for a different application[14] showed that the autoresonant solution was obtained when $\mu > \mu^{th} = 0.411$. Then, by transforming back to our original parameters, we obtain the threshold condition for synchronization by passage through resonance in the driven plasma oscillations problem:

$$\varepsilon > \varepsilon_{th} = 3.8\omega_0^{3/2}\alpha^{3/4}. \tag{27}$$

We find $\varepsilon_{cr}=0.008$ for parameters of simulations in Fig. 4 ($k_0=0.9$, $\alpha=0.000\,15$), which is in excellent agreement with the numerical results.

B. Breather oscillations

Our simulations of synchronized breather oscillations showed that similarly to plasma oscillations, the driving amplitude ε must exceed a threshold for the excitation of a spatially uniform solution in the first stage of formation of breather oscillations. We study this threshold phenomenon in the following. We focus on a weakly nonlinear stage of a spatially uniform solution, where the corresponding Lagrangian (14) is

$$L(u,u_t;t) = \frac{1}{2}(u_t^2 - u^2) + \frac{1}{24}u^4 + \varepsilon \cos \int \omega(t)dt. \quad (28)$$

Applying again Whitham's approach [8], we proceed from the two-scale representation of the solution of our driven problem,

$$u(t) = u_1(t)\cos\,\theta, \quad (29)$$

where θ is the fast angle variable, while $u_1(t)$, $\Omega(t)=\theta_t$, and phase mismatch $\Phi(t)=\theta-\int\omega(t)dt$ are slow. We substitute Eq. (29) into Eq. (28) and average over θ between 0 and 2π. This yields the averaged Lagrangian

$$\Lambda(u_1;\theta,\theta_t) = \frac{1}{2}(\Omega - 1)u_1^2 + \frac{1}{64}u_1^4 + \frac{\varepsilon}{2}u_1\cos\,\Phi, \quad (30)$$

where one assumes proximity to the linear resonance, i.e., $\Omega \approx 1$. Next, we use Λ in the averaged variational principle; take variations with respect to θ and u_1 and obtain the following set of slow evolution equations:

$$u_{1t} = -(\varepsilon/2)\sin\,\Phi, \quad \Phi_t = \alpha t - u_1^2/16 - (\varepsilon/2u_1)\cos\,\Phi. \quad (31)$$

This system is similar to Eqs. (23) and (22) discussed for plasma oscillations above, and, therefore, can be analyzed similarly. By rescaling, $\tau=\alpha^{1/2}t$, $A=\frac{1}{4}\alpha^{-1/4}u_1$, and introducing the complex function $\Psi=A\,\exp(i\Phi)$, Eqs. (31) yield the same nonlinear Shroedinger-type equation (26) for Ψ, where now the parameter is $\mu=\frac{1}{8}\alpha^{-3/4}\varepsilon$. Thus, again, synchronization by passage through resonance in the system takes place for $\mu>0.411$. This, in turn, by returning to our original parameters, yields the following threshold on the driving amplitude for excitation of breather oscillations:

$$\varepsilon_{th} = 3.3\alpha^{3/4}. \quad (32)$$

This completes our analysis of the emergence of synchronized plasma and breather oscillations by passage through resonances in a periodic, driven SG system.

IV. CONCLUSIONS

In conclusion, we have studied the excitation of standing waves of a periodic SG equation by passage through resonances and synchronization. The passage allows efficient excitation and control of large amplitude plasma and breather oscillations in the system by starting from trivial (zero) initial conditions and using a weak $[O(\varepsilon)]$ forcing. Synchronized plasma oscillations were formed by driving the system by a small amplitude standing wave having slowly varying frequency. Efficient excitation of synchronized breather oscillations, in contrast, required driving by a combination of a chirped frequency oscillations and a standing wave. The thresholds for capture into resonance and modulations of slow parameters in the system, oscillating at $O(\varepsilon^{1/2})$ frequencies, are the main signatures of synchronized standing waves. Plasma and breather oscillations studied in this work are the simplest two-phase waves in the periodic SG system. Excitation and control of more general, multiphase SG solutions by passage through resonances seems to comprise an interesting direction for future research. We believe that the inverse scattering transform method [15] yields the proper theoretical framework for studying these most general excitations, similarly to recently studied synchronized multiphase solutions in periodic KdV and NLS systems [1,2]. The simplicity of the forcing used in exciting multiphase solutions in these systems may be a bridge between physics and pure mathematics in the field, making the generation and control of nontrivial multiphase wave forms experimentally realizable.

ACKNOWLEDGMENTS

This work was supported by the US-Israel Binational Science Foundation (Grant No. 2004033), INTAS (Grant No. 03-51-4286), and RFBR (Grant No. 06-02-16058).

APPENDIX: ENERGY E_1 FOR STANDING SG WAVES

By multiplying our driven SG equation (1) by u_t one can rewrite it in the form

$$\left[\frac{1}{2}(u_t^2 + u_x^2) - \cos\,u\right]_t - (u_x u_t)_x = \varepsilon f(x,t)u_t. \quad (A1)$$

Then, for spatially periodic solutions, by averaging in (A1) over one spatial period L, we find

$$dE_1/dt = -\varepsilon\langle f(x,t)u_t\rangle_L, \quad (A2)$$

where the "energy" is defined as

$$E_1 \equiv \left\langle \frac{1}{2}(u_t^2 + u_x^2) - \cos\,u \right\rangle_L + 1. \quad (A3)$$

Therefore, spatially periodic breathers and plasma oscillations of the ideal ($\varepsilon=0$) SG equation conserve E_1, while small ε drive yields a *slow* time variation of E_1. The driven, synchronized standing SG waves described above preserve the form, but slowly change their characteristic parameters to stay in resonance with driving perturbations. Therefore, the calculation of slow "energy" E_1 during the evolution yields useful diagnostics of the excited solution. Next, we relate E_1 to standing wave parameters in the ideal SG case.

We write the standing wave (2) as $u=4\tan^{-1}w$, $w(x,t)=F(x)G(t)$. Then

$$u_t = \frac{4FdG/dt}{1+w^2}, \quad u_x = \frac{4GdF/dx}{1+w^2}.$$

Since, in the ideal SG case, E_1 is independent of time, we can evaluate the average (A3) at any value of $t=t_0$ in $G(t)$. In the case of breather oscillations, $F(x)=A\mathrm{dn}(\beta x,m_1)$ and $G(t)=\mathrm{sn}(\gamma t,m_2)$, and we choose $t_0=0$, so that $G(t_0)$ vanishes. Then $w(x,t_0)=0$, $u(x,t_0)=0$, $u_x(x,t_0)=0$, $dG/dt_0=\gamma\mathrm{cn}(\gamma t_0,m_2)\mathrm{dn}(\gamma t_0,m_2)=\gamma$, and Eq. (A3) yields

$$E_1 = \frac{1}{2}\langle u_t^2 \rangle_L = 8A^2\gamma^2\langle \mathrm{dn}^2(\beta x, m_1)\rangle_L. \quad \text{(A4)}$$

Here we use the functional relation $\mathrm{dn}^2 = 1 - m_1^2\mathrm{sn}^2$ and $\langle \mathrm{sn}^2(\beta x, m_1)\rangle_L = m_1^{-2}[1 - E(m_1)/K(m_1)]$ from [13], to obtain the final result

$$E_1 = 8A^2\gamma^2 E(m_1)/K(m_1). \quad \text{(A5)}$$

In the case of plasma oscillations, $F(x) = A\mathrm{cn}(\beta x, m_1)$ and $G(t) = \mathrm{cn}(\gamma t, m_2)$, and we again choose t_0 such that $G(t_0)$ vanishes [i.e., $\gamma t_0 = K(m_2)$]. Then, similarly to (A4), we find

$$E_1 = 8(dG/dt_0)^2\langle \mathrm{cn}^2(\beta x, m_1)\rangle_L.$$

Using the relations $\mathrm{cn}^2 = 1 - \mathrm{sn}^2$, $d[\mathrm{cn}(\gamma t_0, m_2)]/dt_0 = -\gamma \mathrm{dn}(\gamma t_0, m_2) = -\gamma(1 - m_2^2)^{1/2}$, and the same expression for $\langle \mathrm{sn}^2\rangle_L$ as above, we arrive at

$$E_1 = 8A^2\gamma^2 m_1^{-2}(1 - m_2^2)[m_1^2 - 1 + E(m_1)/K(m_1)] \quad \text{(A6)}$$

for plasma oscillations.

[1] L. Friedland and A. G. Shagalov, Phys. Rev. Lett. **90**, 074101 (2003).
[2] L. Friedland and A. G. Shagalov, Phys. Rev. E **71**, 036206 (2005).
[3] A. Scott, *Nonlinear Science: Emergence and Dynamics of Coherent Structures* (Oxford University Press, Oxford, 1999).
[4] G. L. Lamb, Jr., Rev. Mod. Phys. **43**, 99 (1971).
[5] G. Costabile, R. D. Parmentier, B. Savo, D. W. McLaughlin, and A. C. Scott, Appl. Phys. Lett. **32**, 587 (1978).
[6] A. R. Bishop, M. G. Forest, D. W. McLaughlin, and E. A. Overman, Physica D **23**, 293 (1986).
[7] L. Friedland, Phys. Rev. E **55**, 1929 (1997).
[8] G. B. Whitham, *Linear and Nonlinear Waves* (John Willey, New York, 1973).
[9] L. Friedland, Phys. Rev. E **57**, 3494 (1998).
[10] R. Khomeriki and J. Leon, Phys. Rev. E **71**, 056620 (2005).
[11] C. Canuto, M. Y. Hussaini, A. Quarteroni, and T. A. Zang, *Spectral Methods in Fluid Dynamics* (Springer-Verlag, New York, 1988).
[12] N. Ercolani, M. G. Forest, and D. W. McLaughlin, Physica D **43**, 349 (1990).
[13] E. T. Wittaker and G. N. Watson, *Modern Analysis* (Cambridge University Press, Cambridge, 1927).
[14] E. Grosfeld and L. Friedland, Phys. Rev. E **65**, 046230 (2002).
[15] M. G. Forest and D. W. McLaughlin, J. Math. Phys. **23**, 046230 (1982).